An Adaptive System for Optimal Solar Energy Harvesting in Wireless Sensor Network Nodes

Cesare Alippi, *Fellow, IEEE*, and Cristian Galperti

***Abstract*—The success of wireless sensor networks and their pervasive use is somehow constrained by energy supply which, generally provided by batteries, is a finite resource. Energy harvesting mechanisms must hence be taken into account to grant a long time operational life, with solar energy being the most interesting one in outdoor deployments due to its relatively high power density. In this paper we propose a *low-power* maximum power point tracker (MPPT) circuit *specifically* designed for wireless sensor nodes (hence effective, flexible, low cost and power-aware), i.e., a power transferring circuit for optimally conveying solar energy into rechargeable batteries even in not optimal weather conditions. High efficiency is granted by an ad hoc adaptive algorithm which, by keeping the MPPT electronics in its optimal working point, maximizes energy transfer from the solar cell to the batteries. The suggested implementation is particularly effective in critical weather conditions where traditional solutions do not work and is characterized by a flexible enough design for immediately hosting, in a plug in fashion, different solar panels and battery typologies.**

***Index Terms*—Adaptive algorithms, maximum power point tracker (MPPT) circuits, power converters, solar energy harvesting, wireless sensor networks.**

I. Introduction

THE need of energy harvesting in wireless sensor networks is a primary issue to be tackled to grant effectiveness of the technology in a wide spectrum of applications. In fact, wireless sensor nodes, being mostly planned for outdoor long time operations, only seldom rely on external energy supply sources which, in turn, requires the node to consider energy harvesting mechanisms. In principle, all energy sources should be exploited to extract the available energy; among the others, e.g., see [1]–[5], the solar one is generally the most effective in outdoor applications for the high power density provided and exploitable through solar cells.

Solar cells exhibit a strong nonlinear electrical characteristic, which makes it low effective extracting energy in non stationarity environments. Non stationarity can be associated with changing weather conditions (e.g., cloudy and not optimally radiating solar power environments) and aging effects or efficiency degradation in the solar panel (e.g., dust or rust on the cell surface). Moreover, the energy transfer mechanism is strongly influenced by the illumination condition such as the angle of incidence of the sunlight which varies along the day. All such phenomena can be interpreted as transient or permanent perturbations affecting and reducing the efficiency of the energy production phase.

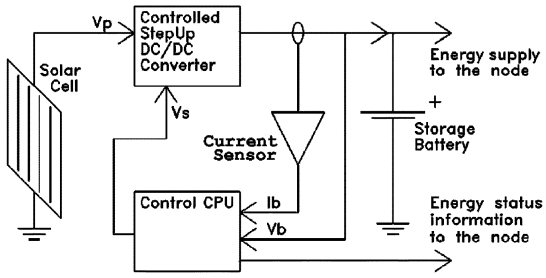

Fig. 1. Schematic design of the MPPT system.

Existing solar energy harvesting solutions for wireless sensor nodes envisage a simple on/off-thresholded charge mechanism relying on a diode connecting the cell with the rechargeable battery [8]. Unfortunately, in a diode- based solution the electrical working point of the cell is fixed and set by the battery voltage, hence preventing any adaptation: whenever the available power is below the threshold the diode disconnects the cell from the battery and no energy is wasted. A diode-based solution is extremely low cost and low power but it suffers from three main drawbacks.

1) The working point of the cell is set by the battery voltage and cannot be adjusted to maximize energy transfer in a changing environment;
2) The threshold prevents the system to operate efficiently at low radiating power rates (i.e., during not optimal solar conditions);
3) The electrical characteristic of the solar cell has to be chosen to properly match the nominal voltage of the battery (hence constraining solar panels and batteries).

All mentioned problems can be addressed by substituting the diode-based circuit with a maximum power point tracker (MPPT) system. Such design philosophy requires the development of an adaptive system to transfer the energy generated by the solar cell into a storage medium, such as a battery or a super capacitor, while maintaining the working point of the cell around the optimal one (for which the transferred power is maximized). Existing MPPT circuits, such as those used for traditional outdoor applications, are not suitable for wireless sensor network nodes; there it is assumed that the generated power is high enough to make negligible the power consumption of the MPPT electronics. Conversely, in wireless sensor

Manuscript received July 14, 2006; revised January 30, 2008. Published July 10, 2008 (projected). This work was supported in part by the IP EU FP6-2005 Wirelessly Accessible Sensors Population (WASP) project and the italian FIRB INtegrated SYstem for EMErgency (INSYEME) project. This paper was recommended by Associate Editor E. Alarcon.

The authors are with the Dipartimento di Elettronica e Informazione, Politecnico di Milano, 20133 Milano, Italy (e-mail: alippi@elet.polimi.it; galperti@elet.polimi.it).

Digital Object Identifier 10.1109/TCSI.2008.922023

1549-8328/$25.00 © 2008 IEEE

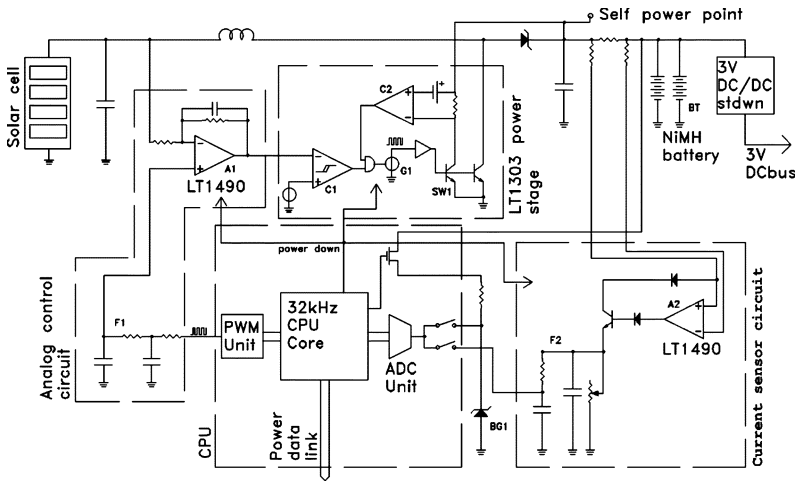

Fig. 2. Detailed design of the MPPT system.

units, the size of the solar panel must be as small as possible and a traditional MPPT circuit would consume, in the best case, all the generated power.

In general, traditional MPPT circuits differentiate themselves in the design of the power converting electronics and/or in the control strategy. Standard buck and boost DC to DC converters as well less traditional series capacitor and mutual inductor configurations have been reported, e.g., see [9]–[11]. The maximum power point detection has been performed with *a priori* modelling of the cell [12], [13], by analog control loops [7], or again, through artificial neural networks and fuzzy solutions [14]. Furthermore, the efficacy of sensing solely the output electric parameters of the converter has been demostrated in [15].

Unfortunately, these solutions do not cope with three main constraints associated with wireless sensor nodes:

1) availability of reduced HW resources on the node;
2) requirement for an extremely low power consumption of the MPPT to allow most of the harvested energy to be conveyed to the battery;
3) extremely low power operation rates.

In this paper, we suggest a novel implementation of an adaptive digitally controlled MPPT circuit especially designed for wireless sensor nodes. The design has been carried out bearing in mind the requests of the embedded target device: extremely low power consumption of the MPPT, fast adaptation to the changing environment, high energy transfer efficiency and low cost.

The structure of the paper is as follows. Section II addresses the issues related to the design of the low power consuming MPPT circuits and its hardware realization; Section III proposes the adaptive digital control technique employed to identify the optimal working point; Section IV finally presents experimental results.

II. Designing a Low-Power, Adaptive Tracking Power Converter System

The designed MPPT circuit is essentially composed of two main logical blocks: 1) a voltage controllable power converter adapting the solar cell with the battery for power transfer; and 2) a control system keeping the solar panel working in the optimal point (the one maximizing the energy harvest). A high level description of the MPPT circuit is given in Fig. 1 while the detailed electronic design is provided in Fig. 2.

The step-up converter stage electronically adapts the solar cell (providing a voltage V_p) with the storage battery (characterized by voltage V_b). *A priori*, voltage V_b differs from V_p being the former dependent and fixed by the battery charge status. Conversely, V_p can be imposed (controlled) leaving to a power $\eta I_p V_p$ transferred to the battery (η is the power converter efficiency). Since V_p can be controlled it is our goal to set V_p to V_m, the voltage for which the trasferred power is maximum (aspects related to the control loop will be given in the next section).

More in detail, the proposed power converter stage is a modified single inductor step up converter built over the LT1303 integrated circuit [17]. The LT1303 natively implements a hysteretic analog control loop designed to stabilize the output voltage by operating its power switch at fixed duty cycle while the entire integrated power stage is turned on and off to control the power flow. This is accomplished by the hysteretic comparator C1 and the square wave generator G1 of Fig. 2.

Moreover, the integrated circuit has an inductor peak current control scheme which avoids the inductor to saturate (the power switch SW1 is composed of two proportional units measuring the inductor current and disabling the switch when the current goes above a maximum nominal value, e.g., 400 mA). This control technique is known to be effective expecially for low power dc–dc stages as it assures high efficiency at low power rates and facilitates the design of the control loop [24]–[26]. This power stage as well as the analog circuit can be forced into an extremely low power consumption state through a dedicated CPU digital signal labelled "power down" in Fig. 2.

The analog control loop implemented by the LT1303, which we suitably modified by introducing a further external operational amplifier A1, grants that V_p *input* is kept at the optimal reference point of voltage V_s. A1 is an extremely low power unit (50-μA supply current) with a reasonable large bandwidth (200-kHz gain–bandwidth product) and provides an amplified control error $V_s - V_p$. The reference signal V_s is digitally provided by the control CPU [20] and needs to be converted into an analog signal. We opted for a pulsewidth modulation

(PWM) technique [instead of a power eager digital–analog converter (DAC)] to perform the digital to analog conversion using a standard PWM modulator provided by the CPU followed by a second order passive low pass filter F1 to generate the analog reference voltage.

Since it was possible to directly connect the reference voltage to one of the high impedance inputs of the LT1490 operational amplifier, no buffer was needed, hence reducing the power consumption of the converter. Battery BT employed for storage is a 300-mAh NiMH rechargeable battery with a nominal voltage of 4.8 V (the battery pack is composed of two 150-mA·h units connected in parallel). We considered NiMH batteries instead of Pb-sealed, NiCd and Lithium-ions ones for their compactness, ease recharge ability and no memory charging effects.

The power delivered to the battery is $P = V_b \cdot I_b$, where I_b is the battery current. To grant a suitable control action both V_b and I_b need to be measured. V_b can be simply acquired through the switched bandgap reference circuit BG1 while I_b requires a more complex procedure since the single inductor step up dc–dc converter provides an output current whose spectra starts at the switching frequency (155 kHz for the LT1303). Moreover, the modified control loop (due to its time delaying PI action) may cause the power converter burst mode switching activity to slow down. This phenomenon might introduce burst mode oscillations on the output current waveform. As such, in order to remove these unwished frequencies, and to provide at the same time an accurate current reading, we employed a high side active current to voltage converter based on op-amp A2 and a second order passive low pass filter F2.

All circuits of the power converter system (LT1303, CPU and LT1490 op-amps) are powered from the "self power point" of Fig. 2, which is located *before* the current reading electronics. As such, the measured current represents the *net* current flowing into the battery (i.e., the total generated current minus that used to power the electronics). This accurate reading allows the CPU for enabling the converter *only* when effective energy harvesting is possible.

III. Adaptive Digital Control Loop

As presented in the previous section the control loop of the MPPT circuit aims at keeping voltage V_p at the optimal reference voltage $V_s = V_m$ maximizing the power transfer from the solar cell to the battery. Since power at the output of the converter is the product of V_b and I_b and the battery voltage can be assumed constant during the control cycle, the stored power is proportional to the output current (here the control requires few seconds while the order of the V_b constant of time is the hour).

Fig. 3 presents two typical behaviours for a solar cell illuminated in two different conditions; the generated current and power as function of the cell voltage V_p are given (in curve A the radiating power is higher than in B). Whatever the technology of the solar cell is (e.g., inorganic or organic), the power versus the cell voltage curve $P(V_p, I_p)$ shows a convex behaviour characterized by a unique maximum associated with the energy transduction phenomenon [16].

De facto, the control algorithm in execution on the CPU has to identify the optimal voltage V_m for which the transferred power

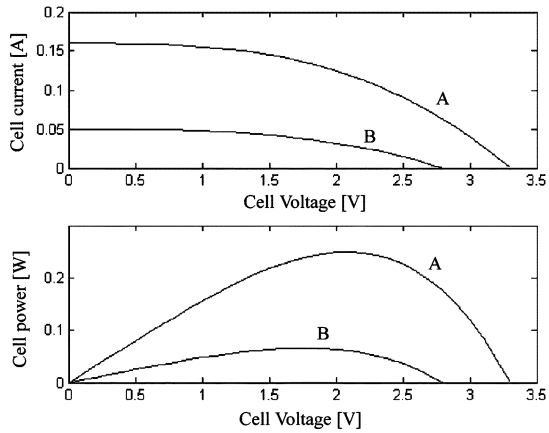

Fig. 3. Solar cell characteristic in two radiating conditions.

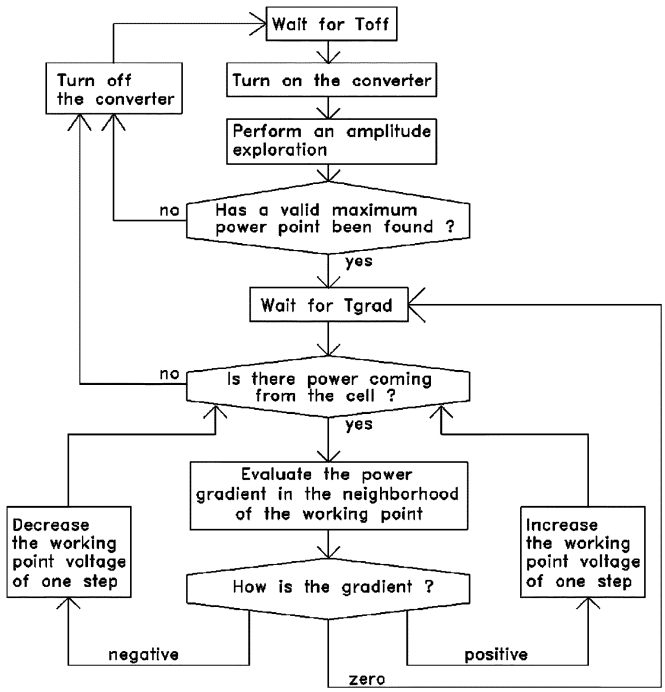

Fig. 4. Control algorithm for identifying and adapting the optimal V_s.

is maximized and, due to changing conditions, track it so that adaptively V_s converges to V_m which, in turn changes over time. The identified optimal V_m at a given time instant will become the reference value to be considered by the analog control loop. Fig. 4 presents a block diagram for the proposed control scheme executed by the CPU.

In its current form, the algorithm providing V_m is a simplified gradient- ascend technique on the $P(V_p, I_p)$ curve w.r.t. V_s (V_s coincides with V_p at the end of the transient phase of the controller). The starting point of the iterative indirect algorithm is provided by a low cost amplitude search technique which periodically scans the power curve in voltage. Starting from the identified sub-optimal point the gradient-ascent algorithm updates V_s to converge towards the optimal point and, once the optimal point neighborhood is reached it tracks environmental changes by modifying V_s accordingly.

Assume the unit starts from a situation without power delivery (e.g., at night). The control CPU is enabled every T_{off} seconds (in our implementation 1 minute) through a polled timing mechanism and, once active, it turns on the converter and scans V_s for identifying a good starting point. This is accomplished by linearly decreasing V_s from a maximum to a minimum value and measure the induced I_b. The voltage associated with the maximum value of I_b is the one considered as starting point for the gradient-ascent algorithm (since V_b can be considered constant during this procedure here we don't need a sophisticated exploration mechanism as differently considered in [19] for a not power-aware MPPT circuit). The gradient control mode is then enabled to track changing weather conditions with a parameterized T_{grad} step update (e.g., 5 s).

Conversely, if no power is generated the CPU turns off the converter and waits for the next wake up signal. More articulate actions, e.g., based on predictive algorithms for optimally setting T_{off} could be envisaged in a future release. The initialization+tracking algorithm must be as simple as possible for power consumption reasons, prompt enough to detect and track changes and flexible to accommodate different solar cells (different typologies of solar panels can be connected without the need of electronic adapters). The described algorithm needs to be simplified in the gradient evaluation, operation costly from the power consumption point of view. In this direction we follow the approach delineated in [7] where only the sign of the gradient is considered (hence resembling a sort of Hebbian rule). The iterative algorithm converges to the correct value provided that the parameter gain amplifying the gradient function is small enough. Moreover, the curvature around the optimal point is rather flat which implies the algorithm to be robust (a small discrepancy between V_s and V_m does not significantly reduce the energy transfer efficiency). Starting from the iterative standard gradient ascend equation

$$\begin{cases} V_{s,i+1} = V_{s,i} + \Delta V_{s,i} \\ \Delta V_{s,i} = \gamma \cdot \left(\frac{d}{dv}(i_{p,i})|_{V_{s,i}} \right) \end{cases} \tag{1}$$

we approximate $\Delta V_{s,i}$ as

$$\hat{\Delta} V_{s,i} = \begin{cases} +\eta, & \text{if } \left(\frac{d}{dv}(i_{p,i})|_{V_{p,i}} \right) > \theta \\ -\eta, & \text{if } \left(\frac{d}{dv}(i_{p,i})|_{V_{p,i}} \right) < -\theta \\ 0, & \text{otherwise} \end{cases} \tag{2}$$

hence obtaining

$$V_{s,i+1} = V_{s,i} + \hat{\Delta V}_{s,i}. \tag{3}$$

Both operations are characterized by an extremely reduced CPU overhead.

To guarantee stability, we kept η at its minimum value, given by the PWM DAC resolution $\eta = 50$ mV. Such a small value reduces the promptness in response time of the control system, which is however acceptable since the maximum adaptation time was 20 s when commuting from a fully sunny situation to a cloudy low-luminosity one. Adaptive solutions cannot be considered in the current system for the power consumption overheads not paid back by an effective energetic gain.

The gradient descent procedure evolves until the gradient becomes null (i.e., it is below threshold θ). If there is not enough energy coming from the solar panel the cell is disengaged, the CPU abandons the tracking modality and returns to the amplitude exploration mode for identifying a new starting point. As such, the algorithm also provides a failure prevention mode against instabilities in the gradient control scheme (which will move the working point outside the limits of the power curve, hence reducing to a null value the power coming from the cell).

The gradient is estimated through its definition, here by superimposing a perturbation wave to the control variable and evaluating its effect on the controlled one. To detect the gradient sign we adopted a correlation operator since a positive correlation stands for a positive power gradient whereas a negative correlation stands for a negative one (and correlation is a straight low-cost operation)

$$X = \sum_{i=1}^{M_p} \frac{|\delta i_b|}{\delta i_b}(i) \cdot \frac{|\delta V_b|}{\delta V_b}(i) \tag{4}$$

where $\delta V_b = V_b(i) - \bar{V}_b$ is the perturbation on the working point superimposed by the CPU, $\delta i_b = i_b(i) - \bar{i_b}$ is the induced perturbation on the controlled variable and M_p is the number of points used to generate the perturbation signal. Parameters θ and M_p, as well as the perturbation waveforms, have been initially identified through SPICE simulations. Afterwards, parameters have been perfected on the field to maximize control loop performances (promptness in reaction and stability) and grant accuracy in current measurements (this aspect will be addressed in more details in subsequent sections).

Finally, the implemented adaptive algorithm can be synthesized as

$$V_{s,i+1} = \begin{cases} V_{s,i} + \eta, & \text{if } X > \theta \\ V_{s,i} - \eta, & \text{if } X < -\theta \\ V_{s,i}, & \text{otherwise.} \end{cases} \tag{5}$$

The frequency and shape of the superimposed perturbations are critical since the converter requires a zero phase transfer function in the perturbing signal spectra to operate correctly (from (4) the converter must not alter the cell power perturbation phase to provide a correct reading). We identified, through numerical simulations, a triangular shape to be a good compromise between signal generation simplicity and frequency requirements. Fig. 5 provides a SPICE simulation of the converter subject to a 2.5-Hz 400-mV peak-to-peak triangle wave superimposed to the working point and the cell characteristic of Fig. 3. Noise affecting the voltage of the cell is due to the parasitic voltage ripple introduced by the converter.

More specifically, the upper plot of Fig. 5 simulates the case where a perturbation is superimposed to the working point in a negative power gradient case. As expected, the controlled variable manifests a negative correlated behaviour with the control variable. Instead, the central plot presents a situation where the

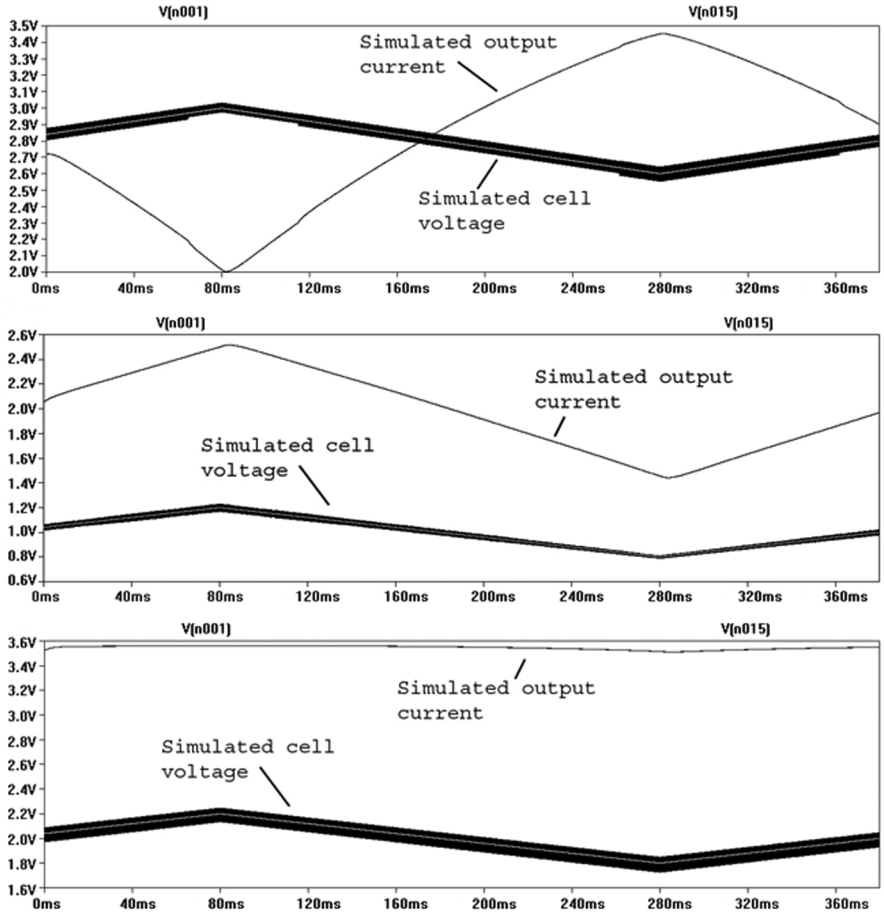

Fig. 5. Converter behavior SPICE simulations with a 2.5-Hz 400-mVpp perturbing wave.

perturbation affects the working point in correspondence with a positive gradient and the controlled variable is positively correlated. Finally, the lower plot shows the situation where the control variable is set to its optimal value and the controlled variable correctly introduces an almost null correlation with the control one. With SPICE circuit simulations we evaluated the effectiveness of (4) once subject to a triangle wave perturbation of 1 s period and 400-mVpp amplitude (which represents the 10% of the estimated working range of the cell voltage). Parameter M_p has been set to 20 (10 points per semiperiod are then used to syntetize the perturbation wave). Finally, θ has been identified through a trial&error procedure so as to guarantee an acceptable level of noise immunity (here we used $\theta = 3$).

We believe that the proposed Hebbian-like tracking algorihtm if effective provided that the following are true.

1) The spectrum of the perturbation wave is limited to the region for which the converter $V_s \rightarrow I_b$ transfer function is flat in modulus with zero phase. Additionally perturbation wave amplitude must allow current channel perturbations arising outside the maximum working point to be separated from noise at the analog–digital converter (ADC) level (satisfaction of this design constraint can be verified at simulation level).
2) The update gain to be used in gradient ascent is small enough to guarantee convergence towards the unique maximum, yet providing enough reaction ability to tracking the changes (the parameters can be identified with simulations and perfected after implementation, as done in this work).

During operational activity the control CPU also monitors the battery voltage and disables the converter whenever the voltage is above a safety voltage threshold (hence introducing an extra charge limiter). Moreover, the CPU performs a digital zero compensation of the current channel readings, sampling the channel before the converter is turned on. This digital zero compensation is necessary since the low current/low power analog current reader has an intrinsic bias which needs to be removed to grant an accurate detection of the zero power condition.

The implemented algorithm runs on a 8 bit PIC16F870 CPU at extra low power 32.768-kHz clock frequency so that the CPU consumes only 30 μA and does not need to be necessarily switched off [20]. The data interface was written in TinyOS [21] so that power-related information necessary to the control CPU can be easily acquired by the master CPU of the WSN node (executing TinyOS code); such information can be fruitfully exploited in energy aware contexts such as routing [22].

IV. Experimental Results

The whole electronics, suitably adapted to be plugged onto a CrossBow Mica2 wireless unit, was implemented and completed with rechargeable batteries and a solar panel. In the following we will consider three amorphous silicon solar cells characterized by 50-, 200-, and 400-mW units, respectively (as

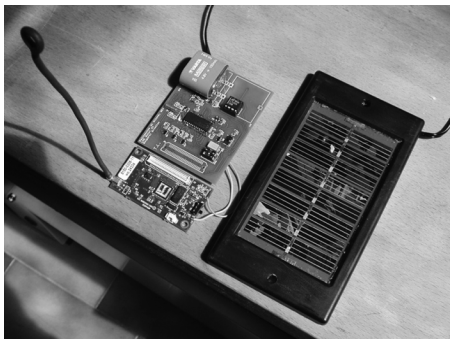

Fig. 6. Solar powered wireless sensor node.

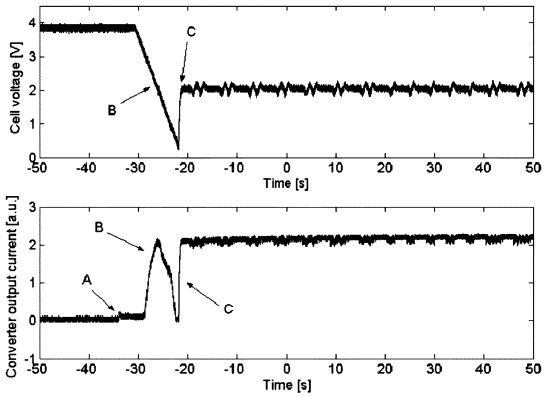

Fig. 7. Amplitude exploration and switch to gradient tracking.

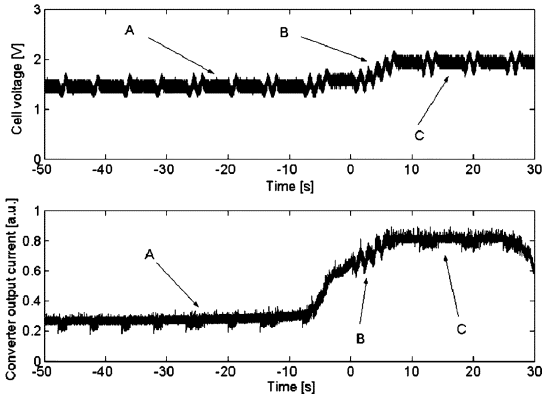

Fig. 8. Adaptive tracking algorithm.

previously said the electronics and the control system are able to host any small power solar panel without any adaptation needs). The suggested WSN unit was then deployed for test in an alpine valley (Italy, north of Como Lake) for more than 100 days starting from the summer of 2005. There, because of the alpine microclimate, thunderstorms, rain, and clouds are the norm rather than the exception; experiments presented in this section must hence to be intended in this operational framework. An operational picture of the WSN unit is given in Fig. 6.

Fig. 7 shows an operational situation where the amplitude exploration is activated to identify the initial operational working point; afterwards the algorithm commutes to the gradient tracking modality. We considered a 50-mW amorphous silicon solar cell. The upper plot of the figure represents the voltage across the cell whereas the lower one the current coming from the converter (proportional to the generated power). The converter is initially off; then the CPU provides a zero-current compensation (point A in the figure), activates the converter and identifies the optimal initial working point through amplitude exploration. This exploration (from the maximum to the minimum value) induces the system to scan the characteristic function of Fig. 3. Such a convex function can be neatly seen in point B. Once this amplitude exploration has been accomplished, the algorithm selects the initial working point associated with the maximum generated power (the maximum value in the plot and the CPU switches into the gradient-based tracking mechanism (point C onwards). The second situation depicted in Fig. 8 represents a case where the adaptive control algorithm takes an active part. The system, once in the control modality, maintains V_s around 1.5 V (point A). The superimposed triangle perturbation waveform can be seen in the control variable but not in the controlled one since the system operates in the optimal working point. In point B we observe that there is a power increment coming from the cell associated with a current increment. This change in radiating power requires V_s to be dynamically updated towards the new optimal point at about 2 V. Such a value is then maintained (point C onward) explaining a stable radiation condition. We appreciate the fact that the system reacts and reaches a stable condition in about 10 s, which we considered to be a good performance in an extremely low power systems (we could easily increase the speed of the controller at the expenses of additional consumed energy).

We generated a realistic situation resembling a node deployment (which depends on the specific application). Here, the node was executing a simple code: 1) acquisition of a sensorial information (the one associated with the energy level); 2) processing (a local sliding window averaging the acquired data); 3) transmission (the processed information was sent to the host every half minute). We positioned the solar panel so that it was receiving only a limited direct radiation (about 3 h per day) being mostly in shadow during the daylight time.

Fig. 9 shows the evolution of the harvested power (upper plot) and its corresponding battery voltage level (lower plot) over 5 days. Here, the power cell is a 400-mW amorphous silicon solar panel.

The system generates a significant amount of power even when the cell is not directly illuminated by the sun (tails A in the figure) and in correspondence with a bad weather (curves B). In particular, the second day was characterized by a strong all-day storm). A zoom of the first day of acquisition is given in Fig. 10. The solid line curve represents the power generated by the cell whereas the dashed one refers to the V_s imposed on the cell by the system. The activation of the control algorithm can be clearly seen: in the early morning the system activates the converter immediately when there is enough power coming from the cell to justify a net gain in energy (the initial working point is set at $V_s = 1.5$ V). Afterwards, the diffuse luminosity rises in intensity and the net transfer of power increases as well. In correspondence with point A the sun directly illuminates the

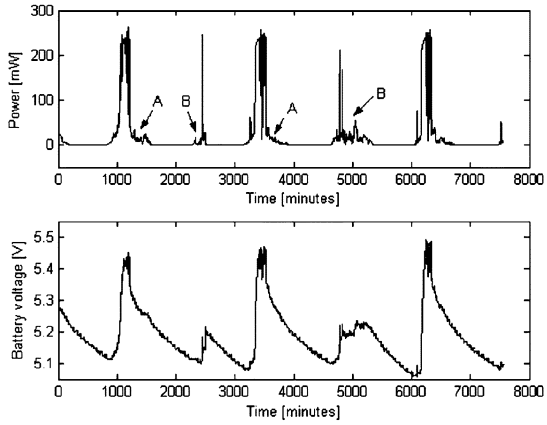

Fig. 9. Acquired power and battery voltage: a 5-day experimentation.

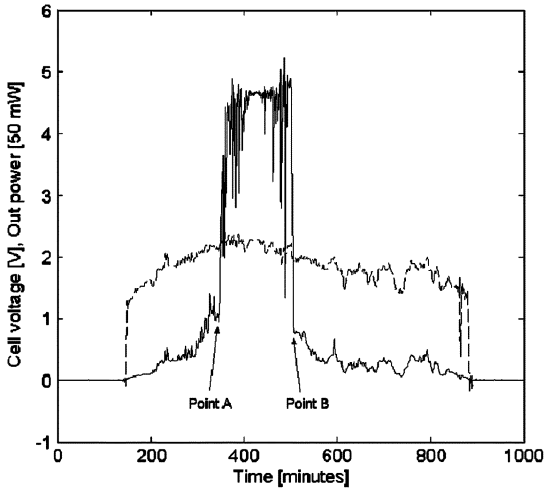

Fig. 10. First day: a zoom.

cell and the power suddenly rises to its maximum value (and V_s stabilizes around 2.2 V). Direct radiation ceases at point B and the panel goes into shadows: V_s is adaptively lowered to extract power also during this non optimal condition. At the sunset, when the CPU identifies not enough power to be generated, the system switches into a sleeping modality which, as we have seen, implies a periodic wake up to control if it is time to return into an energy harvest modality. The effectiveness of the control algorithm can be associated with a good correlation between the produced power pattern and the control voltage one; this is particularly evident in the lower power region, where the adaptive controller is necessary to extract power.

Obviously, the generated energy is simply the integral of the power curve over time. For instance, the total energy generated in Fig. 10 is $E = \int_{T_0}^{T_f} P(t)dt = 2596$ J.

A good figure of merit to evaluate the effectiveness of the proposed system is the percentage of energy generated during shadow periods where traditional solutions are not effective. By considering the [0—point A] interval and from point B onwards we obtain $E_{shadow} = 652$ J which represents a

$$\theta = \frac{E_{shadow}}{E} = 25.1\% \tag{6}$$

of the total energy generated during the day.

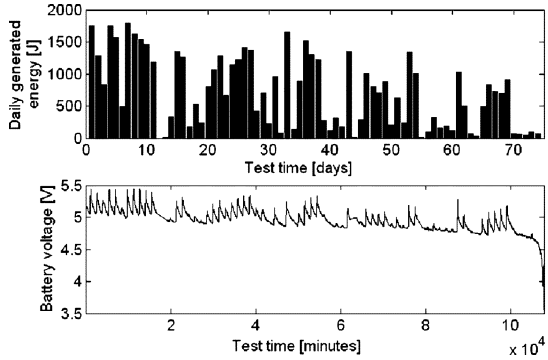

Fig. 11. Acquired energy data and V_b in the 74 days test.

We experimentally discovered that the minimum power for which there it exists a net energy production (available power at the battery minus the one consumed by the electronics) is one 400th of the nominal power for the cell (being around 1 mW in absolute units for the envisaged cell).

A. *Long On-The-Field Deployment*

In order to validate the system in the long run we considered a 200 mW amorphous silicon solar cell (we remind that different solar panels can be directly connected to the electronics without requiring any modification) continuously operating for 74 days (from August 8 2005 to October 20 2005). In this time period we experience, on the alps, a good average weather first, becoming worsening in September and even worsening in October. Moreover, the solar radiation decreases over months getting closer to the winter.

During operational life we acquired and transmitted three sensorial information characterizing the system in its solar energy harvesting ability:

1) cell generated power;
2) cell working voltage V_p;
3) storage battery voltage V_b.

The sample rate was set to 1 acquisition per minute for a total of more than one hundred thousand points. Fig. 11 presents the harvested energy per day (upper plot) and the cell battery voltage (lower plot) over days.

As in the previous experiment the Mica2 mote performed a sliding window average over the acquired data and a subsequent data broadcast towards the base station 24h per day. We verified that, once fully charged, and without any energy harvest mechanism, the system was running out energy after about eight days. Fig. 12 shows the cell's working points during the whole test. We see that the system is experiencing, during its life, all feasible working conditions ranging from 1 to 200 mW. The working voltage is fixed at about 2.2 V when the power rate is above 50 mW where at lower power rates the working points are forced to stay on a convex curve starting at 1.5 V and ending at 2.2 V. We can observe that the working point at high power rates (i.e., above 25% of the nominal power capacity of the cell) is constant but not rigidly imposed as it happens with a diode circuit or an *a priori* given cell model; at low power rates (up to 25% of the nominal power capacity of the cell) the converter adapts to efficiently extract energy.

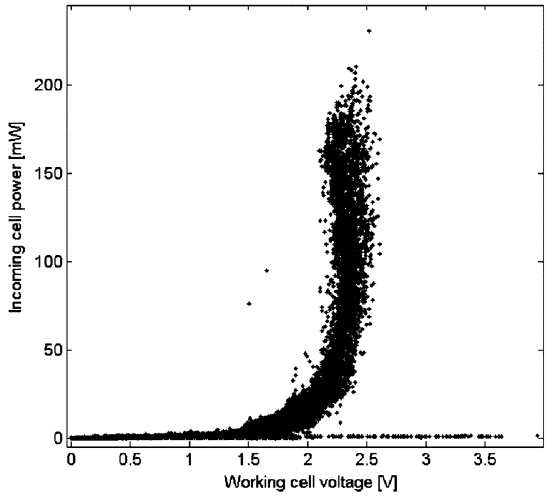

Fig. 12. Cell working points during the whole test.

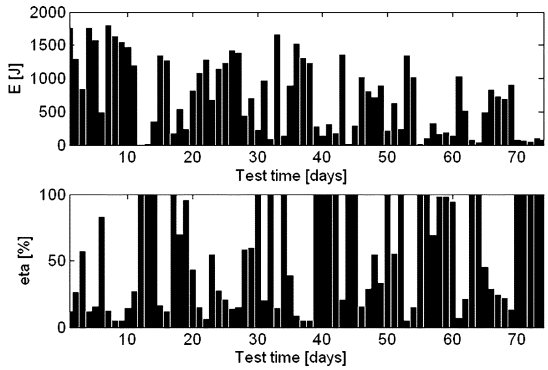

Fig. 13. Generated energy repartition graph.

The effectiveness of the system can be seen by referring to Fig. 13. More specifically, the upper plot represents the daily generated energy which must be compared with the lower plot representing the process efficiency

$$\eta_i = \frac{\int_{\{d_i, P(t)<P_{\rm th}\}} P(t)dt}{\int_{\{d_i\}} P(t)dt} \tag{7}$$

where d_i refers to the ith day time and $P_{\rm th}$ is a pre-set power threshold, which we fixed at 50 mW. De facto, the η plot provides the daily percentage energy generated by the system at low power rates (i.e., below 25% of the nominal power capacity of the cell), characterized by those working points residing on the high curvature of power manifold of Fig. 12 (in these positions a controlled converter is mandatory for an efficient energy generation). It can be seen that this fraction is high not only during days characterized by low energy generation (for which all energy is generated in the low power region, so that η equals 100 %) but also during days characterized by a medium energy generation. Only during days with the highest energy generation (which were prevalently sunny days) this percentage is negligible.

The most relevant information related to the quality of the harvesting process is the overall energy generated in the low power region compared to the total, i.e., the regions where

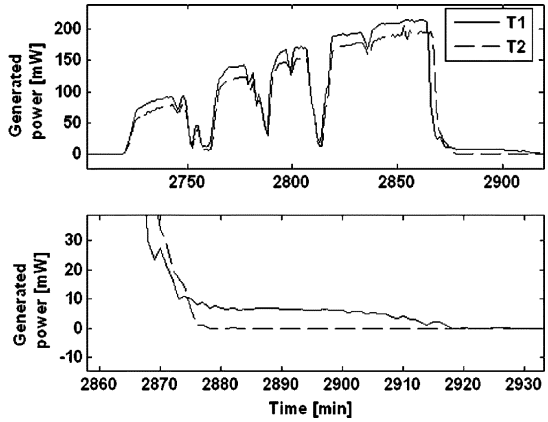

Fig. 14. Comparative experimental results with a 500-mW polycrystalline silicon cell.

the adaptive algorithm is extracting energy otherwise not extractable by a simple diode solution, leads to a

$$\frac{\sum_{i=1}^{74} \eta_i \cdot E_i}{\sum_{i=1}^{74} E_i} = 26.40\%. \tag{8}$$

B. Comparing Traditional and Adaptive Solutions

The last experiments are devoted to compare performance in terms of energy harvested by the suggested adaptive algorithm with the more traditional and—simple one- based on a single diode recharging circuit. In order to carry out comparison with the set up suggested in [8], the proposed MPPT was connected to a 500-mW peak power polycrystalline silicon cell while a second identical cell was connected to a 2.4-V NiMH battery pack through a single diode. The two cells were deployed outdoor, one next the other, in the same environmental conditions. Fig. 14 shows a typical power generation pattern obtained by the two systems. Trace T1 is the power generated by the adaptive system whereas trace T2 is the power generated by the diode circuit.

The power curve generated by the controlled circuit (continuous line) is above the one generated by the diode solution (dotted line) indicating that the former is more effective in transferring energy to the battery than the latter. A zoom of the first plot is given in the lower one and shows that the diode-based circuit does not generate energy at power levels below 10 mW whereas the suggested solution generates energy at power levels as low as 1 mW. We also experimented that the power consumption of the suggested adaptive circuits requires less than 1 mW to operate and that the power stage efficiency is about 50%–60% ; we are currently investigating this issue to further improve performance.

V. Conclusion

A low-power MPPT has been suggested in the paper to maximize the energy generation from a small, low power solar cell. The entire design of the system, from the power converter to the digital control system has been expressly designed for low power operations, independently from the specific nature of the solar panel and the battery type. Experimental results

show that the suggested control system is able to generate an energy transfer rate particularly high also when the cell is in shadow or the weather is cloudy, differently from existing solutions for WSN nodes that do not produce energy in these situations. In future releases we will improve efficiency of the power stage by analyzing and reducing inductor auto oscillations affecting power stage efficiency and by investigating series-parallel cell reconfiguring circuits which can introduce further degrees of freedom in the cell characteristic hence improving the energy harvest possibilities. Furthermore , MPPT algorithm steady-state oscillations will be possibly optimized as suggested in [23].

REFERENCES

[1] G. K. Ottman, H. F. Hofmann, A. C. Bhatt, and G. A. Lesieutre, "Adaptive piezoelectric energy harvesting circuit for wireless remote power supply," *IEEE Trans. Power Electron.*, vol. 17, no. 5, pp. 669–776, Sep. 2002.

[2] A. D. Joseph, "Energy harvesting projects," *IEEE Perv. Comput.*, vol. 4, no. 1, pp. 69–71, Jan.–Mar. 2005.

[3] J. A. Paradiso and T. Starner, "Energy scaveging for mobile and wireless electronics," *IEEE Perv. Comput.*, vol. 4, no. 1, pp. 18–27, Jan. –Mar. 2005.

[4] S. Roundy, E. S. Leland, J. Baker, E. Carleton, E. Reilly, E. Lai, B. Otis, J. M. Rabaey, P. K. Wright, and V. Sundararajan, "Improving power output for vibration-based energy scavengers," *IEEE Perv. Comput.*, vol. 4, no. 1, pp. 28–36, Jan.–Mar. 2005.

[5] C. B. Williams and R. B. Yates, "Analysis of a micro-electric generator for microsystems," in *Proc. 8th Int. Conf. Solid-State Sensors Actuat.*, Jun. 25–29, 1995, vol. 1, pp. 369–372.

[6] C. Hua and C. Shen, "Comparative study of peak power tracking techniques for solar storage system," in *Proc. APEC'98*, Feb. 15–19, 1998, vol. 2, pp. 679–685.

[7] Y. H. Lim and D. C. Hamill, "Synthesis, simulation and experimental verification of a maximum power point tracker from nonlinear dynamics," in *Proc. IEEE 32nd Annu. Power Electron. Specialists Conf.*, Jun. 17–21, 2001, vol. 1, pp. 199–204.

[8] V. Raghunathan, A. Kansal, J. Hsu, J. Friedman, and M. Srivastava, "Design considerations for solar energy harvesting wireless embedded systems," in *Proc. IEEE Int.Conf. Inf. Process. Sensor Netw.*, Apr. 15, 2005, pp. 457–462.

[9] N. K. Lujara, J. D. van Wyk, and P. N. Materu, "Power electronic loss models of DC-DC converters in photovoltaic applications," in *Proc. IEEE Int. Symp. Ind. Electron.* , Jul. 7–10, 1998, vol. 1, pp. 35–39.

[10] M. Veerachary, T. Senjyu, and K. Uezato, "Neural-network-based maximum-power-point tracking of coupled-inductor interleaved-boost-converter-supplied PV system using fuzzy controller," *IEEE Trans. Ind. Electron.*, vol. 50, no. 4, pp. 749–757, Aug. 2003.

[11] J. H. R. Enslin and D. B. Snyman, "Combined low-cost, high-efficient inverter, peak power tracker and regulator for PV applications," *IEEE Trans. Power Electron.*, vol. 6, no. 1, pp. 73–82, Jan. 1991.

[12] J. H. R. Enslin, M. S. Wolf, D. B. Snyman, and W. Swiegers, "Integrated photovoltaic maximum power point tracking converter," *IEEE Trans. Ind. Electron.*, vol. 44, no. 6, pp. 769–773, Dec. 1997.

[13] M. A. S. Masoum, H. Dehbonei, and E. F. Fuchs, "Theoretical and experimental analyses of photovoltaic systems with voltage- and current-based maximum power-point tracking," *IEEE Trans. Energy Conv.*, vol. 17, no. 4, pp. 514–522, Dec. 2002.

[14] C.-Y. Won, D.-H. Kim, S.-C. Kim, W.-S. Kim, and H.-S. Kim, "A new maximum power point tracker of photovoltaic arrays using fuzzy controller," in *Proc. 25th Annu. Power Electron. Specialists Conf.*, Jun. 20–25, 1994, vol. 1, pp. 396–403.

[15] D. Shmilovitz, "On the control of photovoltaic maximum power point tracker via output parameters," *Proc. IEE Elect. Power Appl.* , vol. 152, no. 2, pp. 239–248, Mar. 4, 2005.

[16] T. Markvart, *Solar Electricity*. New York: Wiley, 1994.

[17] "LT1303/LT1303-5 micropower high efficiency dc–dc converters with low battery detector adjustable and fixed 5 V," Linear Technology Corp., Milpitas, CA, datasheet no. LT/GP 0195 10 K, 1995.

[18] "LT1490/LT1491 Dual and Quad Micropower Rail to Rail Input and Output op Amps," Linear Technology Corp., Milpitas, datasheet no. 14901 fb LT/LCG 0600 2K REV B, 1996.

[19] F. Huang, G. Zhimin, T. Forughian, and D. Tien, "A new microcontroller based solar energy conversion modular unit," in *Proc. Power Conv. Conf.* , Aug. 3–6, 1997, vol. 2, pp. 697–700.

[20] "PIC16F870 28/40-Pin, 8-Bit CMOS FLASH Microcontrollers," Microchip Technology Corp., Chandler , AZ, datasheet no. DS30569B, 2003.

[21] "TinyOS project official website," Univ. California, Berkeley, CA, 2008 [Online]. Available: http://www.tinyos.net

[22] A. Kansal and M. Srivastava, "An environmental energy harvesting framework for sensor networks," in *Proc. ACM Int. Symp. Low Power Electron. Design*, 2003, pp. 481–486.

[23] N. Femia, G. Petrone, G. Spagnuolo, and M. Vitelli, "Optimization of perturb and observe maximum power point tracking method," *IEEE Trans. Power Electron.*, vol. 20, no. 4, pp. 963–973, Jul. 2005.

[24] B. Arbetter and D. Maksimovic, "Control method for low-voltage DC power supplies in battery-powered systems with power management," in *IEEE PESC Rec.*, 1997, pp. 1198–1204.

[25] E. Alarcón, G. Villar, F. Guinjoan, and A. Poveda, "Quasi-optimum efficiency in output voltage hysteretic control for a buck switching converter with wide load range," in *Proc. IEEE Power Electron. Specialists Conf.*, 2005, pp. 2118–2125.

[26] B. Bryant and M. K. Kazimierczuk, "Modeling the closed-current loop of PWM boost. DC-DC converters operating in CCM with peak. Current-mode control," *IEEE Trans. Circuits Syst. I, Reg. Papers*, vol. 52, no. 11, pp. 2404, 2412, Nov. 2005.

Cesare Alippi (SM'94–F'05) received the Dr.Ing. degree in electronic engineering (*summa cum laude*) and the Ph.D. degree in computer engineering from Politecnico di Milano, Milan, Italy, in 1990 and 1995, respectively.

He has completed research work in computer sciences at the University College, London, U.K., and the Massachussets Institute of Technology, Cambridge. Currently, he is a Full Professor in Information Processing Systems at the Politecnico di Milano. His research interests include application level analysis and synthesis methodologies for embedded systems, neural networks, and wireless sensor networks. His research results have been published in more that 120 technical papers in international journals and conference proceedings.

Cristian Galperti received the Dr.Ing. degree in electronic engineering (*summa cum laude*) from Politecnico di Milano, Milan, Italy, in 2004. Currently, he is a Ph.D. student at the Politecnico di Milano where he is investigating wireless sensor networks issues (expecially energy harvesting and sensor acquisition) and embedded systems for personal safety and homeland security.